ACS APPLIED ENERGY MATERIALS

www.acsaem.org

Article

Factorial Design and Optimization of Trimetallic CoNiFe-LDH/Graphene Composites for Enhanced Oxygen Evolution Reaction

Daniele Alves,* Gillian Collins, Marilia B. Dalla Benetta, Eithne Dempsey, Jae-Jin Shim, Raj Karthik, and Carmel B. Breslin

Cite This: ACS Appl. Energy Mater. 2025, 8, 5455−5467

Read Online

ACCESS | Metrics & More | Article Recommendations | Supporting Information

ABSTRACT: Layered double hydroxides (LDH) have exhibited promising applications as electrocatalysts in oxygen evolution reactions (OER). In this work, trimetallic LDHs (CoNiFe-LDH) were designed and grown on graphene (G) through a one-step hydrothermal approach to obtain a structure that promotes efficient charge transfer. A 2-level full-factorial design was utilized to evaluate the effects of varying the concentrations of Co (1.5, 3, and 4.5 mmol) and graphene (10, 30, and 50 mg) on the OER activity. The potential needed to deliver 10 mA cm^{-2} was chosen as the response parameter. The independent and dependent parameters were fitted to a linear model equation through ANOVA analysis. The computed *p*-values were below 0.05 signifying the statistical significance of the concentrations of cobalt and graphene and their interaction, suggesting a correlation with the OER activity. The OER experiments were conducted in triplicate using the $Co_{[3]}Ni_{[3]}Fe_{[3]}$-LDH/$G_{[30]}$ (central point) to estimate variability (0.58%). Comparative analysis showed that $Co_{[1.5]}Ni_{[3]}Fe_{[3]}$-LDH/$G_{[10]}$ achieved the lowest onset potential (1.54 V), potential at 10 mA cm^{-2} (1.58 V), and Tafel slope (58.4 mV dec^{-1}), indicating that a low concentration of cobalt and graphene make an efficient electrocatalyst for OER. Furthermore, the optimized composite demonstrated favorable electronic properties, with a charge transfer resistance (R_{CT}) of 188.1 Ω, and exhibited good stability, maintaining its catalytic activity with no significant loss over a 24-h period.

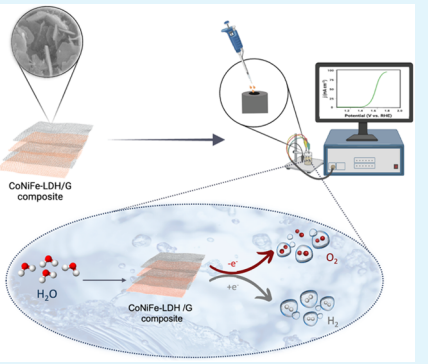

KEYWORDS: *layered double hydroxide, graphene, electrocatalyst, factorial design, oxygen evolution reaction*

1. INTRODUCTION

For many decades, fossil fuels, such as gas, oil, and coal, have acted as the primary contributors to electricity generation.[1] Nevertheless, the combustion of carbon-based fuels causes substantial emissions of greenhouse gases, notably carbon dioxide (CO_2), thereby triggering climate change and adversely affecting human well-being and the environment.[2] Consequently, there is an endeavor to curtail the utilization of fossil fuels and channel investments into renewable energy modalities, such as solar, wave, and wind power. Despite their environmental merits, these renewable sources are characterized by intermittency, making them incapable of ensuring a consistent energy supply.[3] Consequently, increasing their proportion in the energy grid poses a big challenge. Thus, it is important to innovate and develop efficient and environmentally acceptable energy sources.

The oxygen evolution reaction (OER) constitutes a pivotal half-reaction within diverse renewable energy technologies. These include water electrolysis,[4] metal-air batteries,[5] and fuel cells.[6] Essentially, it involves the conversion of water (H_2O) into molecular oxygen (O_2) through a four-electron transfer process. Despite its significance, the OER is intrinsically sluggish and energy-intensive, necessitating the advancement of electrocatalysts that are both efficient and stable to facilitate this reaction.[7] Notably, noble metal-based materials, including IrO_2 and RuO_2, have shown superior OER performance under alkaline conditions.[8] Nonetheless, their use is limited by high costs and limited reserves. Hence, the strategic design of novel electrode materials featuring low cost, high conductivity, and minimal overpotential assumes a crucial role in advancing electrocatalysis.

In recent years, layered double hydroxides (LDH) have gained recognition as possible candidates for the OER due to their cost-effectiveness, tunable composition, and favorable electrocatalytic properties.[9] Ni-based LDHs, particularly NiFe-LDH, have been extensively studied and demonstrated as efficient OER electrocatalysts in alkaline environments.[10] Due to its optimal adsorption energy for hydroxide anions, NiFe-LDH is recognized as a very good electrocatalyst for OER.[11] However, its limited electrical conductivity hinders further enhancement of its OER catalytic activity.[12] Meanwhile, Co-

Received: February 17, 2025
Revised: March 31, 2025
Accepted: April 2, 2025
Published: April 7, 2025

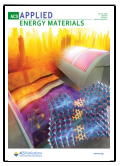

based LDHs, such as NiCo-LDH[13] and CoFe-LDH[14] have been proven to have excellent electrocatalytic activity.

In contrast to binary LDHs, the ternary LDHs, incorporating diverse transition elements can exhibit higher capacitance and contain more abundant active sites.[15] Introducing a third metal ion in binary LDHs can alter the electronic structure and improve the conductivity, thereby increasing the density of active sites and facilitating more efficient electron transfer.[16] Notably, Co-doping of NiFe-LDH, with vertical orientation, interconnections, and uniform distribution, has been shown to effectively enhance its electrocatalytic performance.[17]

Nevertheless, the utilization of LDH electrode materials is limited by their low conductivity and tendency for agglomeration. These challenges can be mitigated through the integration of LDH with carbon materials which exhibit good conductivity,[18] and this includes graphene (G),[19] carbon fibers,[20] carbon nanotubes (CNT),[21] and carbon cloth (CC).[22] Graphene serves as an excellent substrate for catalyst immobilization in electrocatalysis, attributed to its remarkable electrical conductivity, large surface area, and impressive stability.[23] This enhances the quantity of active sites, consequently improving electrochemical performance.[24] Therefore, the combination of ternary LDHs, characterized by reversible redox activity, with conductive graphene is anticipated to offer a promising strategy for developing hybrid materials with superior OER activity, facilitated by the advantageous interplay between LDHs and graphene.[25]

Accordingly, in this work, the concentrations of cobalt and graphene, which serves as the carbon source, were optimized using a full-factorial design to formulate CoNiFe-LDH/G composites, aiming to enhance OER performance through an economical and efficient single-step hydrothermal reaction. This optimized composite was characterized and used as an electrocatalyst for the OER. Its performance was compared with the corresponding bimetallic components. This innovative approach employs statistical analysis to improve the efficiency of material preparation, leading to enhanced OER performance. Additionally, to the best of our knowledge, CoNiFe-LDH combined with graphene nanoplatelets has not previously been explored as an electrocatalyst for OER.

2. EXPERIMENTAL SECTION

2.1. Materials. The cobalt ($Co(NO_3)_2{\cdot}6H_2O$), nickel ($Ni(NO_3)_2{\cdot}6H_2O$) and iron salts ($Fe(NO_3)_3{\cdot}9H_2O$), urea (NH_2CONH_2), graphene nanoplatelets and RuO_2 were all obtained from Sigma-Aldrich, UK. A glassy carbon electrode (GCE, 3 mm diameter) was used as a support for the CoNiFe-LDH/G composites.

2.2. Synthesis of $Co_{[m]}Ni_{[3]}Fe_{[3]}$-LDH/$G_{[n]}$ Composites. The $Co_{[m]}Ni_{[3]}Fe_{[3]}$-LDH/$G_{[n]}$ composites were synthesized using a hydrothermal method. The Ni and Fe content was maintained constant, while the amounts of graphene and Co were varied to give different molar ratios of Co to Ni and Fe (Co:Ni:Fe = 0.5:1:1 or 1:1:1 and 1.5:1:1). The Co and graphene levels were varied to investigate their combined effects on the OER activity. Experimentally, these composites were synthesized according to the procedures developed in the previous works,[14,26−28] using a 2-level full factorial design, as illustrated in Table 1. The graphene nanoplates (10, 30, or 50 mg, Table 1) were dispersed in a 10 mL solution of deionized water and ethanol (equal volumes), and then sonicated for 20 min. A second solution containing $Co(NO_3)_2$ at different concentrations (1.5, 3, or 4.5 mmol, Table 1), combined with 3 mmol of $Ni(NO_3)_2$, and 3 mmol of $Fe(NO_3)_3$ in 20 mL of deionized water was prepared. Then, a third solution was obtained by dissolving 1.5 g of urea in 10 mL of deionized water. All three solutions were mixed, followed by stirring for 1 h to ensure complete dissolution. The resulting mixture was

Table 1. Factors and Levels for the Optimization of the CoNiFe-LDH/G Composites

composites	1st factor [Co]	2nd factor [G]	[Co] mmol	[G] mg
$Co_{[1.5]}Ni_{[3]}Fe_{[3]}$-LDH/$G_{[10]}$	−1	−1	1.5	10
$Co_{[4.5]}Ni_{[3]}Fe_{[3]}$-LDH/$G_{[10]}$	+1	−1	4.5	10
$Co_{[1.5]}Ni_{[3]}Fe_{[3]}$-LDH/$G_{[50]}$	−1	+1	1.5	50
$Co_{[4.5]}Ni_{[3]}Fe_{[3]}$-LDH/$G_{[50]}$	+1	+1	4.5	50
$Co_{[3]}Ni_{[3]}Fe_{[3]}$-LDH/$G_{[30]}$	0	0	3	30

carefully transferred into a 100 mL Teflon-lined stainless-steel autoclave and maintained at 120 °C for 12 h. The $Co_{[m]}Ni_{[3]}Fe_{[3]}$-LDH/$G_{[n]}$ composites were washed several times with ethanol and deionized water, collected and then dried at 60 °C for 18 h. To verify the elemental composition, X-ray energy-dispersive spectroscopy (EDX) was conducted in triplicate for all composites, with the results summarized in Table 2. The elemental composition of the $Co_{[m]}Ni_{[3]}Fe_{[3]}$-LDH/$G_{[n]}$ composites (Table 2) aligns with the precursor concentrations (Table 1), reflecting controlled Co and graphene (%C) variation while maintaining constant Ni and Fe (standard deviation <0.8%). Additionally, to evaluate the influence of each component on the electrochemical performance and OER activity, a series of control materials with different compositions were synthesized using the same method, and named CoNiFe-LDH, NiFe-LDH/G, CoNi-LDH/G, and CoFe-LDH/G.

2.3. Characterization. The optimized $Co_{[m]}Ni_{[3]}Fe_{[3]}$-LDH/$G_{[n]}$ and its graphene-free counterpart, $Co_{[m]}Ni_{[3]}Fe_{[3]}$-LDH, were chosen for further investigation through structural characterization and electrochemical analysis. X-ray photoelectron spectroscopy (XPS) (Kratos AXIS ULTRA spectrometer) was conducted using monochromatic Al Kα radiation (1486.58 eV, 300 W, 20 mA, 15 kV) to determine surface element composition and valence state of the as-synthesized composite. The sample morphologies were examined via field emission scanning electron microscopy (FE-SEM, Hitachi S-4800), while the elemental composition was analyzed using energy-dispersive X-ray spectroscopy (EDX, Oxford Instrument INCAz-act ESX system). X-ray diffraction (XRD) analysis was conducted using a Powder X-ray PANalytical X'Pert-PRO MPD system to investigate the crystal structure of the samples. The measurements were performed with Cu Kα radiation (λ = 1.5406 Å) at an operating voltage of 40 kV, while the composites were also analyzed by Fourier transform infrared spectroscopy (FTIR, Nicolet iS50 FTIR spectrometer) in the range 4000−500 cm^{-1}. The potential leaching of Co, Ni and Fe from the LDH composite was analyzed using inductively coupled plasma mass spectrometry (ICP-MS) (7900 ICP-MS, Agilent, Japan). The plasma was generated using argon gas (99.99% purity) with a 15 L min^{-1} plasma flow rate, while the auxiliary and nebulizer gases were supplied at 1 L min^{-1}.

2.4. Electrochemical Measurements. The OER activity of the LDH electrocatalysts was studied at a polished and thoroughly cleaned GCE. The GCE was polished sequentially with 1 and 6 μm Akasol diamond suspensions on an Aka−Napel microcloth, followed by thorough rinsing with deionized water, sonication in deionized water and dried under an air flow. The LDH catalyst ink was formulated by mixing 3 mg of the LDH with 0.5 mL deionized water and 0.5 mL ethanol, followed by sonication for 10 min to ensure homogeneity. The resulting ink was applied to the GCE via drop casting, achieving an approximate catalyst loading of 84.9 μL cm^{-2}.

The electrochemical measurements were carried out in 1 M KOH (pH 13.6) in a three-electrode cell, with the LDH-modified GCE, a silver/silver chloride (Ag/AgCl) reference, and a high surface area platinum wire counter electrode. Linear sweep voltammetry (LSV) was conducted at a scan rate of 5 mV s^{-1}. All potentials were converted to the reversible hydrogen electrode (RHE) scale (E_{RHE} =

https://doi.org/10.1021/acsaem.5c00483
ACS Appl. Energy Mater. 2025, 8, 5455−5467

Table 2. Composition in % Atomic of the CoNiFe-LDH/G Composites

composites	Co % atomic[a]	Ni % atomic[a]	Fe % atomic[a]	C % atomic[a]	O% atomic[a]
$Co_{[1.5]}Ni_{[3]}Fe_{[3]}$-LDH/$G_{[10]}$	4.3 ± 0.5	5.9 ± 0.4	6.4 ± 0.5	38.6 ± 2.1	44.8 ± 2.7
$Co_{[4.5]}Ni_{[3]}Fe_{[3]}$-LDH/$G_{[10]}$	9.3 ± 0.9	5.6 ± 0.7	6.1 ± 0.6	37.5 ± 1.9	41.5 ± 2.5
$Co_{[1.5]}Ni_{[3]}Fe_{[3]}$-LDH/$G_{[50]}$	4.0 ± 0.5	5.8 ± 0.7	6.3 ± 0.6	48.1 ± 2.6	35.8 ± 2.2
$Co_{[4.5]}Ni_{[3]}Fe_{[3]}$-LDH/$G_{[50]}$	8.9 ± 0.7	5.6 ± 0.6	6.3 ± 0.8	47.4 ± 2.4	31.8 ± 2.1
$Co_{[3]}Ni_{[3]}Fe_{[3]}$-LDH/$G_{[30]}$	5.8 ± 0.6	5.7 ± 0.5	6.2 ± 0.7	42.8 ± 2.4	39.5 ± 2.6

[a]Mean ± standard deviation (n = 3).

$E_{Ag/AgCl}$ + 0.197 V + 0.059 × pH) and were *iR*-corrected. Current densities were normalized to the geometric surface area of the GCE. Electrochemical impedance spectroscopy (EIS) measurements were performed over a frequency range of 1 × 10^6 to 0.007 Hz at 1.58 V (RHE) using a 10 mV perturbation potential. The obtained impedance data were fitted to an equivalent circuit model to determine the charge transfer resistance. In addition, the stability of the selected trimetallic LDH, $Co_{[m]}Ni_{[3]}Fe_{[3]}$-LDH/$G_{[n]}$, was evaluated over a 24 h-period under a constant applied potential of 1.58 V (RHE). Following the 24 h polarization period, the EIS response of the LDH was measured and compared to the response of the freshly prepared LDH. Additionally, to assess the stability of the composite under conditions relevant to scaled-up electrochemical systems, which generally require higher current densities, a chronoamperometry experiment was conducted at a constant potential of 1.66 V (RHE), equivalent to 50 mA cm^{-2} for 72 h-period.

2.5. Statistical Analysis. Linear models were employed to analyze the OER response variable, incorporating replication as a factor with three levels. A linear response surface accounting for Co and G concentrations in the linear predictor for the mean was employed. The interaction effect of Co and G concentrations on the potential required to achieve 10 mA cm^{-2} was evaluated using F-tests. A contour plot was generated to illustrate the predicted OER value over a continuous 2D grid for varying concentrations of Co and G.

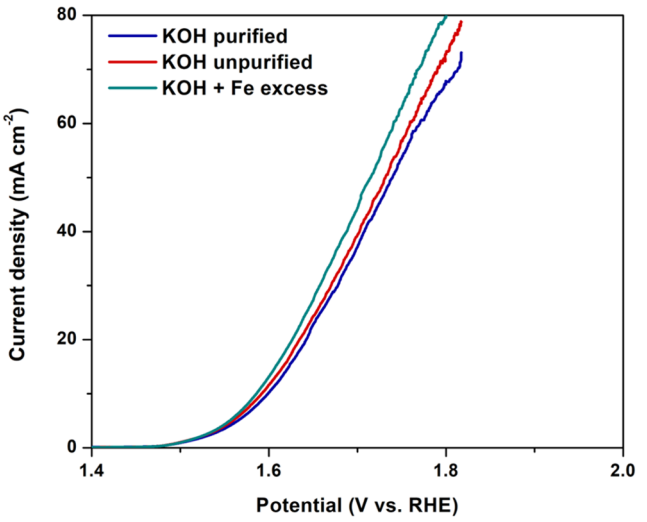

Figure 1. OER polarization curves using $Co_{[1.5]}Ni_{[3]}Fe_{[3]}$-LDH/$G_{[10]}$ in 1 M KOH solution, in purified, unpurified, and Fe-excess conditions.

3. RESULTS AND DISCUSSION

3.1. Alkaline Electrolyte Preparation and Evaluation. Alkaline aqueous electrolytes, such as KOH and NaOH, are crucial for energy devices, including electrolyzers, fuel cells, supercapacitors, and batteries.[29] Recent findings have shown that Fe impurities can notably impact the OER performance of Ni-based electrocatalysts.[30] Therefore, addressing impurities is vital to assess alkaline electrolyte quality for objective evaluation and comparison of electrochemical energy systems. Based on this, CoNiFe-LDH/G was initially employed for OER in 1 M KOH solutions in unpurified, supplemented with excess Fe (20 ppm) and purified conditions to assess the effect of Fe ions on the electrocatalytic performance of the LDH composite. For the purification process, the method developed by Marquez et al.[31] was employed, in which Fe ions are adsorbed onto the surface of insoluble $Ni(OH)_2$. It is evident in Figure 1 that the presence or excess of iron did not impact the onset potential or the current at the lower overpotentials. However, it did have a slight impact at the higher current densities, particularly above 50 mA cm^{-2}. Consequently, the CoNiFe-LDH/G composites were studied and statistically optimized at 10 mA cm^{-2} in the commercial KOH solution as the purification process is costly and time-consuming for large-scale operations due to the numerous steps and chemicals involved.

3.2. Selection of the $Co_{[m]}Ni_{[3]}Fe_{[3]}$-LDH/$G_{[n]}$ Composite. Factorial design is a useful approach for studying how different parameters affect the optimization of a specific process. In the context of a full-factorial experimental design, measurements of responses are conducted across the complete array of combinations formed by varying the levels of the experimental parameters. For this study, a 2-level full-factorial design was used to evaluate the influence of cobalt and graphene concentrations (independent parameters) on the performance of the NiFe-LDH. The potential equivalent to a current density of 10 mA cm^{-2} during the OER (dependent variable), was the chosen response parameter. Five combinations of dependent variables were used in the optimization experiments. The polarization curves and Tafel slopes of the $Co_{[m]}Ni_{[3]}Fe_{[3]}$-LDH/$G_{[n]}$ composites for OER are shown in Figure 2a,b, respectively. Additionally, the OER activity was studied in triplicate using the $Co_{[3]}Ni_{[3]}Fe_{[3]}$-LDH/$G_{[30]}$ (central point) to estimate the variability, which was determined at 0.58%, indicating a low variability.

As shown in Figure 2a,b, the $Co_{[1.5]}Ni_{[3]}Fe_{[3]}$-LDH/$G_{[10]}$ provides the best OER activity when compared with the other composites that have higher Co and G concentration levels. An impressive onset potential of 1.54 V, combined with a potential of 1.58 V to generate 10 mA cm^{-2}, and a Tafel slope of 58.4 mV dec^{-1} were achieved for the $Co_{[1.5]}Ni_{[3]}Fe_{[3]}$-LDH/$G_{[10]}$. This highlights the important roles of both cobalt and graphene when designing the optimum electrocatalyst. Interestingly, lower concentrations of Co are preferable, and this may be connected with the development of Co-containing particles with the higher Co contents.[32] While the presence of graphene may be beneficial with the carbon providing sites for adsorption of the OH^- ions,[33] an excess concentration may lead to agglomeration of the graphene sheets giving poorer dispersion of the transition metal centers, decreasing the number of active sites for catalysis.[34]

https://doi.org/10.1021/acsaem.5c00483
ACS Appl. Energy Mater. 2025, 8, 5455−5467

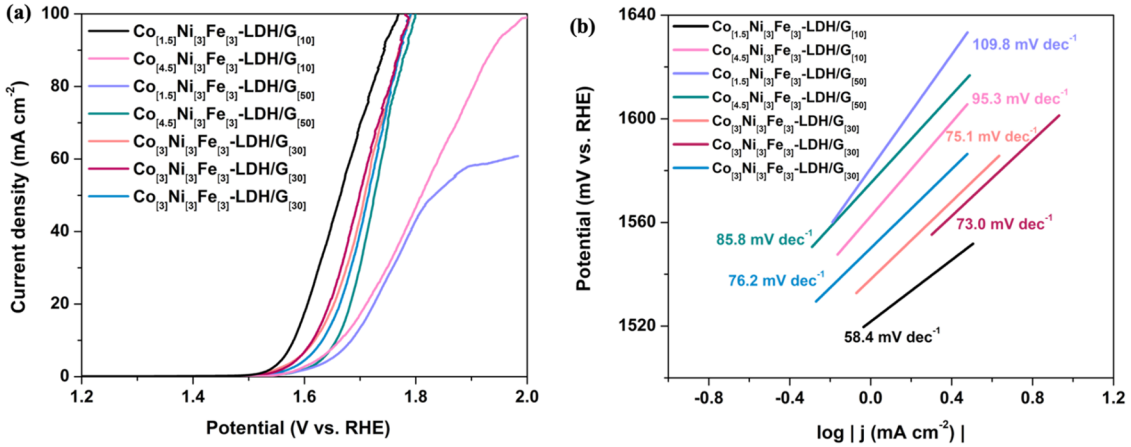

Figure 2. (a) The OER LSV curves of the composites synthesized with different molar ratios of $Co(NO_3)_2$ and amounts of graphene. (b) Tafel slopes derived from the LSV curves.

To assess the reproducibility of the OER performance using the synthesized composites, all experiments were carried out in triplicate. The corresponding standard deviations (<5%) are reported in Table 3, indicating a high level of experimental consistency and reliability. To determine the impact of the main factors on the OER, the independent and dependent parameters were fitted to the linear model equation. ANOVA analysis was conducted at a 95% confidence level, and the corresponding results are presented in Table 4.

Table 3. Potential at 10 mA cm^{-2} with RSD for the Synthesized Electrocatalysts

catalyst	potential at 10 mA cm^{-2} (V)[a]	RSD (%)
$Co_{[1.5]}Ni_{[3]}Fe_{[3]}$-LDH/$G_{[10]}$	1.58 ± 0.02	2.11
$Co_{[4.5]}Ni_{[3]}Fe_{[3]}$-LDH/$G_{[10]}$	1.67 ± 0.01	1.42
$Co_{[1.5]}Ni_{[3]}Fe_{[3]}$-LDH/$G_{[50]}$	1.69 ± 0.01	1.53
$Co_{[4.5]}Ni_{[3]}Fe_{[3]}$-LDH/$G_{[50]}$	1.67 ± 0.02	2.34
$Co_{[3]}Ni_{[3]}Fe_{[3]}$-LDH/$G_{[30]}$	1.62 ± 0.01	1.36

[a]Mean ± standard deviation (n = 3).

Table 4. A Summary of the ANOVA Tests with the Significance of the Variables

source		F-value	p < 0.05	remarks
model		17.4	0.005	significant
[Co]		9.5	0.009	significant
[G]		18.7	0.004	significant
[Co][G]		25.0	0.003	significant
model S	0.01			
R^2	0.97			
adjusted R^2	0.92			

A satisfactory prediction regression model, with high determination coefficient values of R^2 = 97.2%, and R^2(adj) = 91.6%, was obtained, confirming that the ANOVA test is validated. The p-values are less than 0.05, indicating that the parameters and their interactions are significant, while the F-values confirm that the model is significant (p < 0.05). In particular, the model terms indicate that the cobalt and graphene concentrations and their interactions, are significant, implying that the OER activity is correlated to these parameters. It was also confirmed by the Pareto plot of effects, illustrated in Figure 3a, that the main effects, cobalt concentration and amount of graphene, and their interaction are significant at a 5% significance level. The response data were fitted to a linear regression equation, according to eq 1, where the potential is expressed in units of V vs RHE and corresponds to the potential required to deliver 10 mA cm^{-2} of current density.

$$\text{Potential} = 1.5025 + 0.1050[\text{Co}] + 0.003750[\text{G}] - 0.002500[\text{Co}]^*[\text{G}] - 0.02500\text{CtPt} \quad (1)$$

Here, CtPt corresponds to the central point, [Co] indicates the concentration of cobalt, [G] gives the graphene amounts, and the term [Co]*[G] represents the level of interaction between Co and G. Based on eq 1, it can be confirmed that there is a linear correlation between the factors and the response, with the potential increasing as the cobalt concentration and mass of graphene increases, making the electrocatalysts less favorable for the OER. On the other hand, the interactions between the cobalt and graphene contribute to lowering the potential. This indicates that lower concentrations of Co and graphene are more favorable. Indeed, this can be seen in the 2D contour plot, in Figure 3b, which shows the main and interaction effects of the dependent variables on the potential at 10 mA cm^{-2}. This confirms the relationship between the cobalt concentration and the amount of graphene, with the optimum combinations with Co concentrations between 1.5 and 2.25 mM and G between 10 and 20 mg. Therefore, the $Co_{[1.5]}Ni_{[3]}Fe_{[3]}$-LDH/$G_{[10]}$ was selected as the optimized material for further investigations. To elucidate the contribution of each element to the OER activity, control materials were synthesized and analyzed systematically.

3.3. Characterization of the Optimized LDH Composite. In addition to the characterization of the LDH composite, the incorporation of graphene into the LDH was investigated. A combination of XPS, FE-SEM, XRD, and FTIR analyses was employed in the characterization studies, and to elucidate the structural and morphological changes induced by the addition of graphene.

The chemical composition, and valence states of the $Co_{[1.5]}Ni_{[3]}Fe_{[3]}$-LDH/$G_{[10]}$ are summarized in the XPS spectra shown in Figure 4. The XPS survey spectrum, Figure 4a, confirms the presence of Fe, Ni, Co, O and C. The Co 2p spectra in Figure 4b, display two peaks at 781.6 eV (Co^{2+}

https://doi.org/10.1021/acsaem.5c00483
ACS Appl. Energy Mater. 2025, 8, 5455−5467

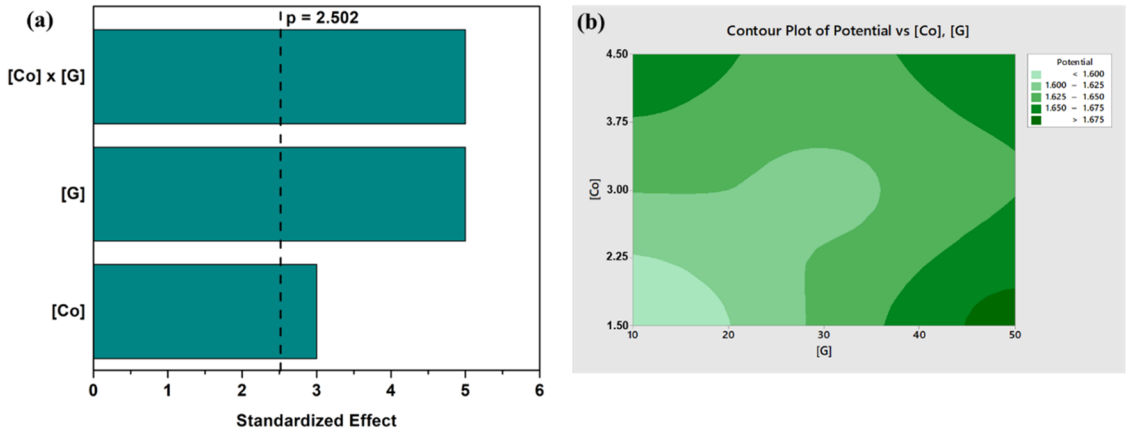

Figure 3. (a) Pareto plot of the standardized effects of 2^2 full-factorial design (response is potential at 10 mA cm^{-2}; $\alpha = 0.05$); and (b) 2D contour plot of potential at 10 mA cm^{-2} as a function of cobalt concentration and amount of graphene.

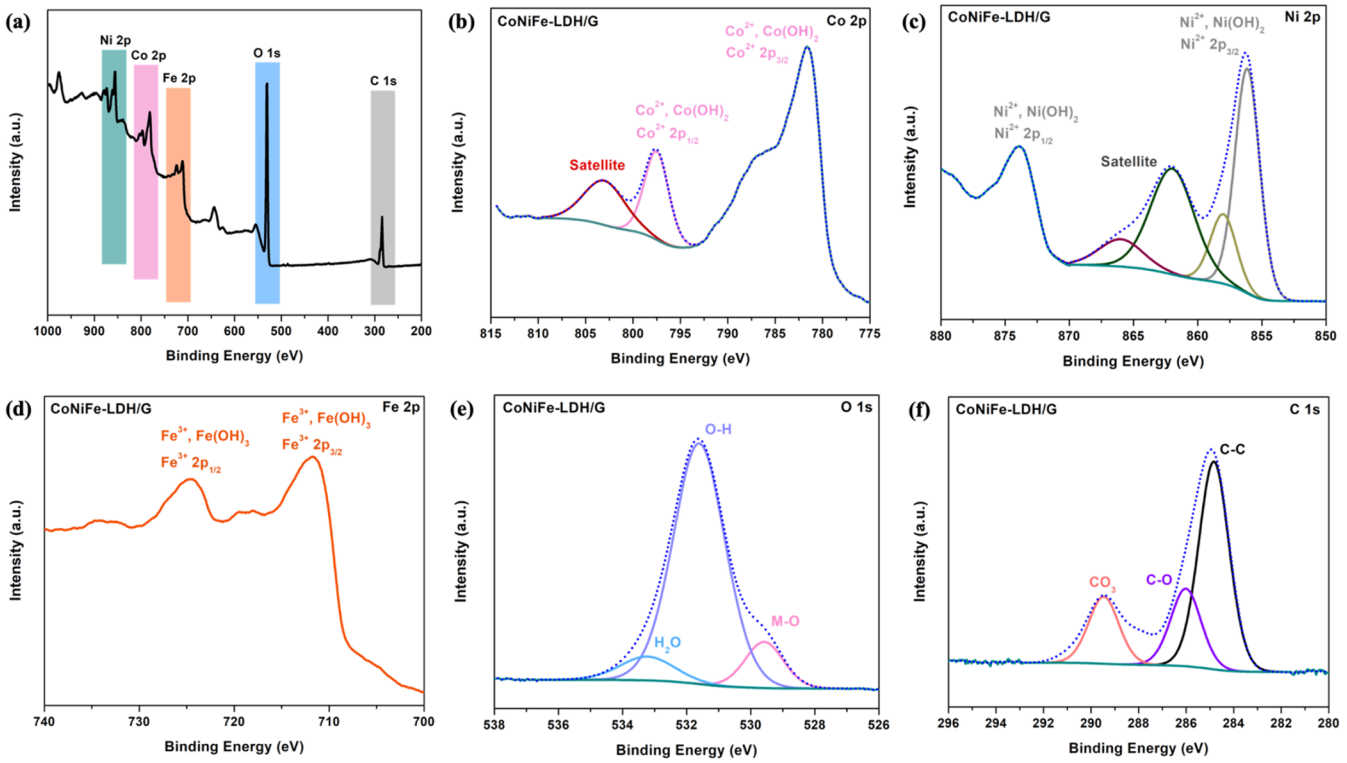

Figure 4. XPS of $Co_{[1.5]}Ni_{[3]}Fe_{[3]}$-LDH/$G_{[10]}$ (a) Survey, (b) Co 2p, (c) Ni 2p, (d) Fe 2p, (e) O 1s, and (f) C 1s.

$2p_{3/2}$) and 797.5 eV, (Co^{2+} $2p_{1/2}$), along with a satellite peak at 803.0 eV, confirming the presence of the Co^{2+} species.[35] The Ni 2p spectra in Figure 4c show characteristic peaks at 856.1 and 874.3 eV, corresponding to the Ni^{2+} $2p_{3/2}$ and Ni^{2+} $2p_{1/2}$ energy states, respectively. This is consistent with the Ni^{2+} species within $Ni(OH)_2$.[36] Additional satellite peaks are seen at 862.0 and 866.0 eV, and these suggest the formation of NiO[37] at the surface. In Figure 4d, two peaks at 711.0 and 724.9 eV corresponding to Fe^{3+} $2p_{3/2}$ and Fe^{3+} $2p_{1/2}$, are evident, and this is consistent with previous studies.[38,39]

In Figure 4e, the O 1s spectrum reveals two peaks at 529.6 and 531.6 eV, corresponding to M-O and O−H, respectively. These peaks suggest the formation of hydroxyl interlayer ions in the trimetallic LDHs;[40] while the peak at 533.2 eV is associated with adsorbed water.[41] In the C 1s spectrum shown in Figure 4f, a peak at 284.5 eV is identified with C = C and C−C bonds, while another peak at 286.0 eV corresponds to C−O, confirming the successful incorporation of graphene.[42] Furthermore, a peak at 290.8 eV in the C 1s spectra, corresponds to CO_3, which may originate from reaction byproducts,[43] or indicate the presence of intercalated carbonate anions. Collectively, the peaks observed in the spectra for these constituent elements provide evidence for the successful synthesis of the intended trimetallic LDH composites, forming a heterogeneous architecture. Additionally, XPS analysis was performed on the $Co_{[1.5]}Ni_{[3]}Fe_{[3]}$-LDH composite (Figure S1) to assess the chemical interactions between the LDH and graphene. Notably, a slight narrowing of the peak at 531.6 eV related to M-O bonds upon graphene addition is observed on comparing Figures 4e and S1d. The slight narrowing, around 1/4 of the M-O peak width, in the XPS spectra of graphene-incorporated LDHs can be attributed

https://doi.org/10.1021/acsaem.5c00483
ACS Appl. Energy Mater. 2025, 8, 5455−5467

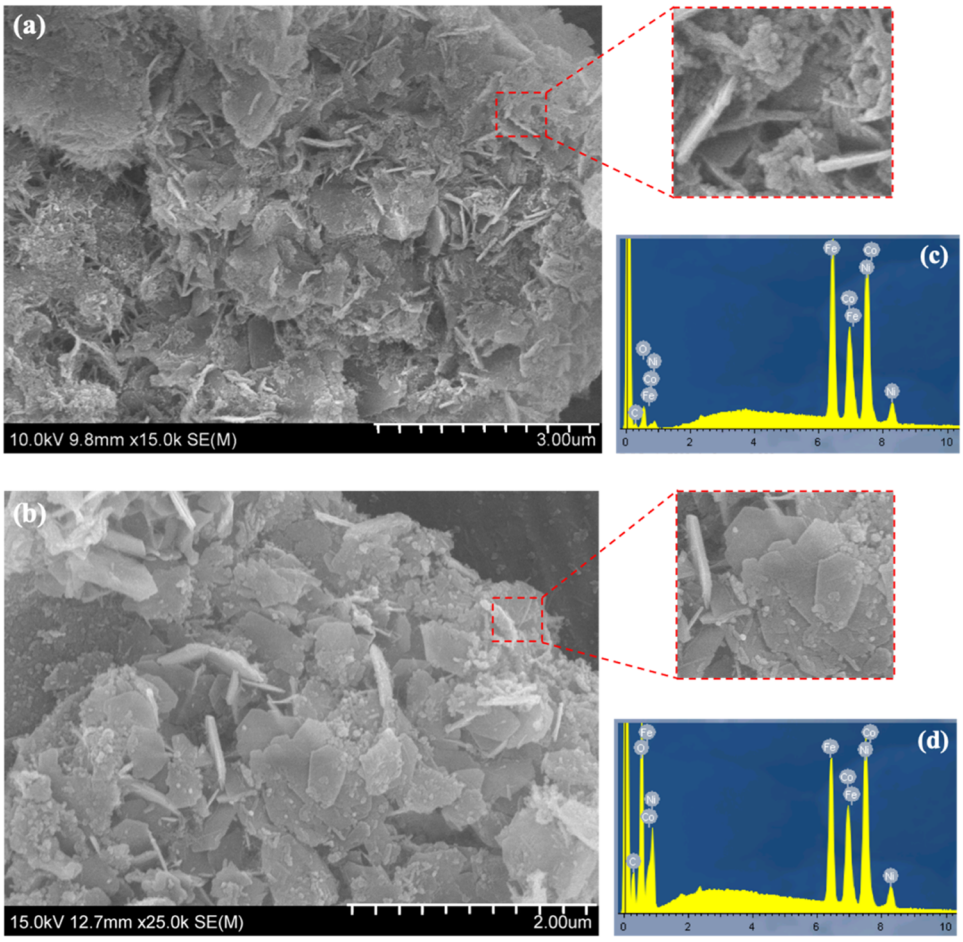

Figure 5. FE-SEM images of (a) CoNiFe-LDH and (b) $Co_{[1.5]}Ni_{[3]}Fe_{[3]}$-LDH/$G_{[10]}$ EDX spectra for (c) CoNiFe-LDH and (d) $Co_{[1.5]}Ni_{[3]}Fe_{[3]}$-LDH/$G_{[10]}$.

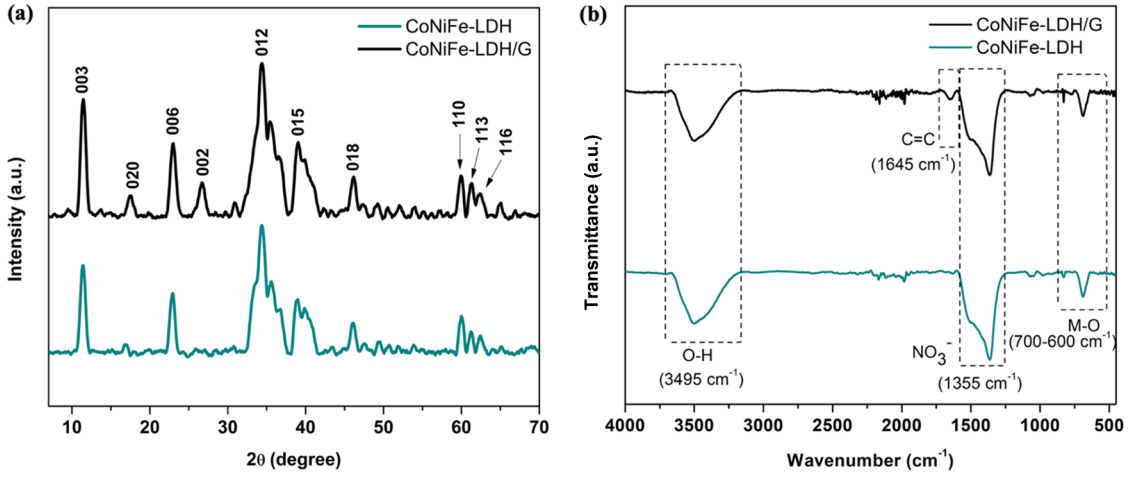

Figure 6. (a) XRD and (b) FTIR spectra of CoNiFe-LDH and $Co_{[1.5]}Ni_{[3]}Fe_{[3]}$-LDH/$G_{[10]}$.

to electronic interactions between graphene's π-electron system and the LDH structure, causing subtle charge redistribution around the metal centers and altering their local electronic environment.[44] Furthermore, the incorporation of graphene can enhance structural organization by reducing defects and improving uniformity, resulting in a more homogeneous chemical environment.[25] In contrast, the XPS spectra of metal hydroxides showed no noticeable changes, likely due to their stable structure, which prevents significant interaction with graphene. This lack of interaction results in no discernible alterations in their XPS profiles.[45] The combined effects observed in the LDH-graphene composite, such as the narrowing of the M-O peak, indicate structural modifications that suggest the successful incorporation of graphene into LDHs. This structural enhancement contributes to improved stability and performance of the composite.

https://doi.org/10.1021/acsaem.5c00483
ACS Appl. Energy Mater. 2025, 8, 5455−5467

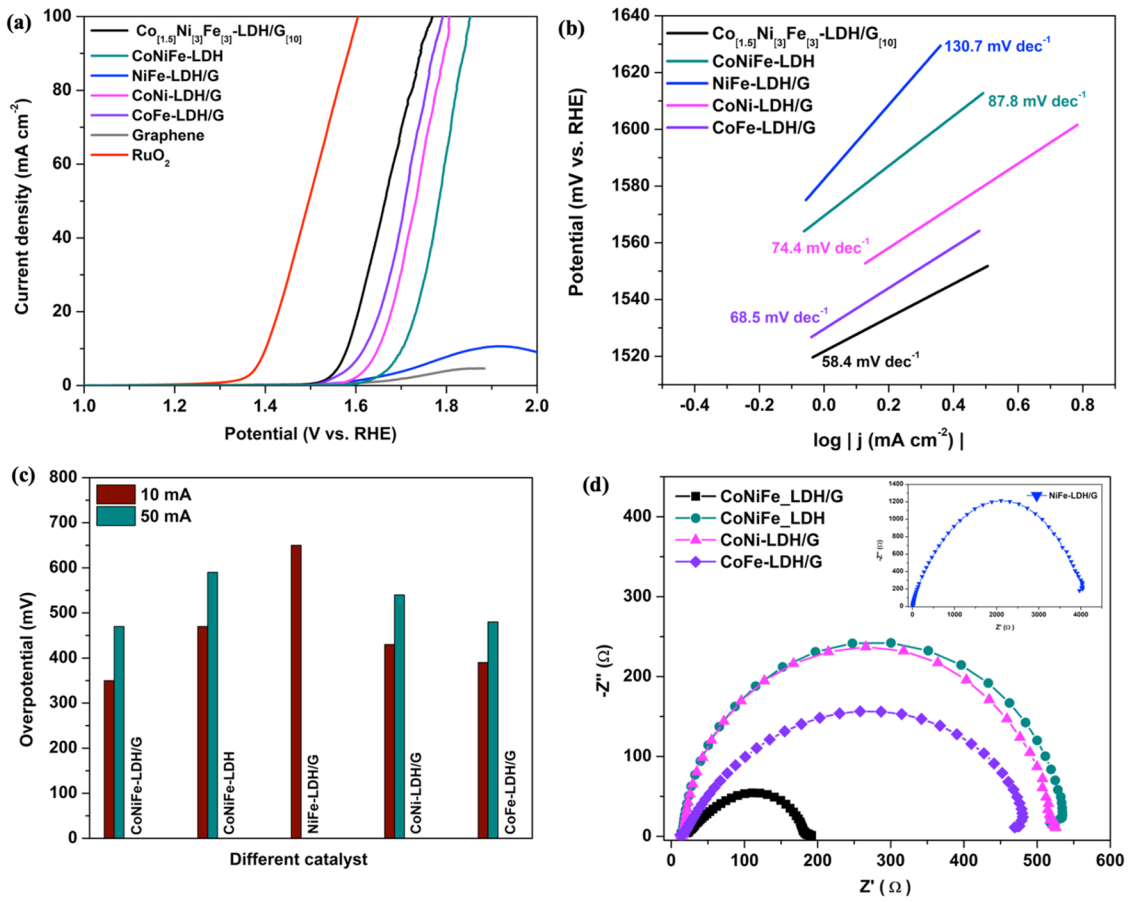

Figure 7. (a) The OER LSV curves, (b) Tafel slopes derived from the LSV curves, (c) histogram of overpotentials at 10 and 50 mA cm^{-2}, and (d) electrochemical impedance plots recorded in 1 M KOH.

The morphological changes induced by graphene incorporation were further examined using FE-SEM, as shown in Figure 5. The surface of CoNiFe-LDH, Figure 5a, exhibits a characteristic two-dimensional flake structure. The compact CoNiFe-LDH flakes intersect, giving rise to the formation of clusters, and exhibit a vertical arrangement, in accordance with recent experimental observations.[46] Furthermore, the CoNiFe-LDH nanosheets are stacked layer by layer, exhibiting a compact arrangement, which results in a dense surface coating. The morphology modification of the trimetallic surface with the insertion of graphene can be observed in Figure 5b. The metal layer of CoNiFe-LDH is positively charged, while the graphene nanoplates are negatively charged.[47] Hence, electrostatic attraction facilitates the adsorption of graphene onto the CoNiFe-LDH surface, leading to the formation of the LDH-G coating with graphene nanoplatelets covering its surface − a characteristic structure of graphene.[35,48] Furthermore, examination of the sectional FE-SEM image of CoNiFe-LDH and $Co_{[1.5]}Ni_{[3]}Fe_{[3]}$-LDH/$G_{[10]}$ reveals a close attachment and coverage of graphene on the surface of $Co_{[1.5]}Ni_{[3]}Fe_{[3]}$-LDH/$G_{[10]}$. This is consistent with the data in Table 1, where the *p*-values indicate a significant interaction between the Co and G.

The EDX spectra, in Figure 5c,d, suggest that the main elements on both LDH surfaces are Co, Ni, Fe and O, confirming the successful development of the CoNiFe-LDH. However, the $Co_{[1.5]}Ni_{[3]}Fe_{[3]}$-LDH/$G_{[10]}$, Figure 5d, exhibits a higher relative carbon and oxygen concentration, compared to CoNiFe-LDH (Figure 5c). This is associated with the insertion of graphene sheets, which are decorated with oxygen-containing functional groups, such as C−O groups and oxygen vacancies,[49] into the LDH which is beneficial in the transfer of electrons from the LDH to graphene.[50]

Crystallographic analysis via XRD provided further insights into the structural integration of graphene with the LDH, as presented in Figure 6a. The XRD pattern of CoNiFe-LDH shows diffraction peaks at 2θ = 11.5, 17.6, 23.4, 34.4, 38.9, 46.2, 59.9, 61.5, and 62.6° which can be indexed to the (003), (020), (006), (012), (015), (018), (110), (113), and (116) planes of the LDH phase.[17,51] This is a clear indication of the successful synthesis of CoNiFe-LDH. The XRD of the $Co_{[1.5]}Ni_{[3]}Fe_{[3]}$-LDH/$G_{[10]}$ shows a similar diffraction pattern. However, an additional weak peak at 27.26° is seen, corresponding to the (002) plane of graphene.[48,52] This confirms the successful formation of $Co_{[1.5]}Ni_{[3]}Fe_{[3]}$-LDH/$G_{[10]}$.

FTIR spectroscopy was used to obtain further chemical insight into the $Co_{[1.5]}Ni_{[3]}Fe_{[3]}$-LDH/$G_{[10]}$ and the corresponding graphene-free CoNiFe-LDH. The FTIR spectra were recorded between 4000 and 500 cm^{-1}, and typical plots are illustrated in Figure 6b. A broad absorption band is evident at 3495 cm^{-1}, and this corresponds to the O−H stretching vibrations of the interlayer H_2O molecules and is typical of LDHs.[53] The vibration mode of the NO_3^- ions in the interlayer is evident at 1355 cm^{-1}.[54] The bands observed from 600−700 cm^{-1} are attributed to M−O, M−O−M and O−M−O vibrations where M corresponds to Co, Ni and Fe.[55,56] Compared with CoNiFe-LDH, the FT-IR spectrum of the $Co_{[1.5]}Ni_{[3]}Fe_{[3]}$-LDH/$G_{[10]}$ shows an extra weak absorption

https://doi.org/10.1021/acsaem.5c00483
ACS Appl. Energy Mater. 2025, 8, 5455−5467

band at 1645 cm^{-1} which is related to the vibration of C = C at graphene,[57,58] and this confirms that the graphene nanoplatelets were successfully incorporated throughout the LDH structure.

Overall, the combined XPS, FE-SEM, XRD and FTIR analyses demonstrate that graphene incorporation into the $Co_{[1.5]}Ni_{[3]}Fe_{[3]}$-LDH structure is facilitated by electrostatic attractions and chemical interactions between functional groups, resulting in enhanced structural stability and potentially improved OER activity.

3.4. Electrocatalyst Performance. The OER activity of the $Co_{[1.5]}Ni_{[3]}Fe_{[3]}$-LDH/$G_{[10]}$, and the two-component control samples, NiFe-LDH/G, CoNi-LDH/G and CoFe-LDH/G were studied and compared to the RuO_2 benchmark catalyst. The resulting LSV curves are presented in Figure 7a. While RuO_2 demonstrates a lower onset potential of 1.38 V, the optimized $Co_{[4.5]}Cu_{[3]}Fe_{[3]}$-LDH/$G_{[10]}$ catalyst shows a comparable onset potential and similar slope, suggesting promising electrochemical behavior. The onset potential and overpotential at 10 mA cm^{-2} (Figure 7c) were selected as the basis for characterizing the catalytic performance of the materials, and these are summarized in Table 5. It can be observed that the optimized $Co_{[1.5]}Ni_{[3]}Fe_{[3]}$-LDH/$G_{[10]}$ shows the lowest onset potential at 1.54 V corresponding to an overpotential of 350 mV. The NiFe-LDH/G demonstrates the highest onset potential at 1.67 V with an overpotential of 650 mV, highlighting the significant role of cobalt in enhancing the OER performance. This can be attributed to the oxidation of Ni^{2+} to Ni^{3+} promoted by the Co charge transfer effect which in turn gives the higher conductivity NiOOH phase.[59] Additionally, NiOOH activates the Fe sites which are inaccessible to electron transfer in the $Ni(OH)_2$ phase.[17,60] Meanwhile, the Fe^{3+} ions promote the oxidation of Co^{2+} to Co^{3+}, forming CoOOH which further improves the OER activity for the $Co_{[1.5]}Ni_{[3]}Fe_{[3]}$-LDH/$G_{[10]}$ composite.[61] Furthermore, CoNiFe-LDH shows a higher onset potential at 1.64 V with an overpotential of 470 mV compared to $Co_{[1.5]}Ni_{[3]}Fe_{[3]}$-LDH/$G_{[10]}$, suggesting that the added graphene ensures an adequate electron supply during the electrocatalytic process, thereby boosting the OER performance.[62]

Table 5. Onset Potential and Overpotential for the Different Composites

composites	onset potential (V)	overpotential (mV)
$Co_{[1.5]}Ni_{[3]}Fe_{[3]}$-LDH/$G_{[10]}$	1.54	350
CoNiFe-LDH	1.64	470
NiFe-LDH/G	1.67	650
CoNi-LDH/G	1.63	430
CoFe-LDH/G	1.58	390

A comparative analysis with studies from the recent literature, as shown in Table 6, demonstrates that the $Co_{[1.5]}Ni_{[3]}Fe_{[3]}$-LDH/$G_{[10]}$ exhibits a lower overpotential at 10 mA cm^{-2}. This suggests that its electrocatalytic performance is either superior or at least comparable to other reported electrocatalysts for OER. This improved performance can be attributed to the in situ growth of CoNiFe-LDH on the graphene substrate, which effectively mitigates the restacking of graphene sheets and prevents the aggregation of LDH particles. This structural integration fosters strong interactions and synergistic effects between the CoNiFe-LDH and graphene, facilitating enhanced electron transfer and consequently leading to superior electrocatalytic efficiency.[63]

Table 6. Performance Comparison of the Optimized LDH with the Literature

composites	KOH electrolyte (M)	overpotential at 10 mA cm^{-2} (mV)	ref.
CoAl-LDH/NG	1.0	365	64
N-NiZnCu- LDH/rGO	1.0	489	42
CoNiMn- LDH/PPy/rGO	0.1	369	65
CoAl-LDH	1.0	415	64
NiCe-LDH/CNT	1.0	417	66
ZnCo-LDH/rGO	0.1	450	67
NiMn-LDH	1.0	520	68
CO_3−CoAl-LDH	1.0	422	69
benzoate-Co-LDH	1.0	360	70
Mo-NiFe-LDH	1.0	491	71
ZnCo-LDH	1.0	420	72
$Co_{[1.5]}Ni_{[3]}Fe_{[3]}$-LDH/$G_{[10]}$	1.0	350	this work

Additional insights into the kinetics and mechanism of the OER were obtained using Tafel analysis. The Tafel equation is described in eq 2, where the slope (b) determines how rapidly the current density (i) increases with an increase in overpotential (η), while the constant (a) depends on the exchange current density. The LSV curves are presented in Figure 6a, while the Tafel regions and the associated slopes are shown in Figure 6b.

$$\eta = a + b \log(i) \tag{2}$$

A low Tafel slope of 58.4 mV dec^{-1} was obtained for the $Co_{[1.5]}Ni_{[3]}Fe_{[3]}$-LDH/$G_{[10]}$, Figure 7b. This combined with the low overpotential relative to the other LDHs, Table 4, indicates that this optimized system has an electronic structure that permits more efficient adsorption/desorption of the oxygenated species, giving rise to a higher OER activity.[73] Additionally, the CoNiFe-LDH without graphene has a much higher Tafel slope of approximately 94.5 mV dec^{-1}, clearly highlighting the significant role of graphene in the $Co_{[1.5]}Ni_{[3]}Fe_{[3]}$-LDH/$G_{[10]}$ composite.

Further information on the electronic conductivity of the composites was obtained using electrochemical impedance spectroscopy (EIS). The equivalent circuits employed for fitting the impedance data are shown in Figure S2 and involve the solution resistance, (R_s), charge transfer resistance (R_{CT}) and a constant phase element (CPE). The impedance of the $Co_{[1.5]}Ni_{[3]}Fe_{[3]}$-LDH/$G_{[10]}$ composite can be fitted to a simple Randles cell, while an additional constant phase element is required with the NiFe-LDH/G. The plots are characterized by a depressed semicircle, Figure 7d. The diameter of the semicircle, which corresponds to the R_{CT}, varies considerably depending on the nature of the LDHs. Cearly the $Co_{[1.5]}Ni_{[3]}Fe_{[3]}$-LDH/$G_{[10]}$ composite has the lowest charge transfer resistance.

The R_{CT} values for the various LDH composites are compared in Table 7. Clearly, the $Co_{[1.5]}Ni_{[3]}Fe_{[3]}$-LDH/$G_{[10]}$ exhibits the lowest R_{CT}, at 188.1 ± 4.58 Ω, and this is consistent with its lower onset potential, lower overpotential and favorable Tafel slope. Indeed, the R_{CT} obtained for $Co_{[1.5]}Ni_{[3]}Fe_{[3]}$-LDH/$G_{[10]}$ is around 20 times lower compared to NiFe-LDH/G, which has the highest R_{CT} of

https://doi.org/10.1021/acsaem.5c00483
ACS Appl. Energy Mater. 2025, 8, 5455−5467

Table 7. Electrochemical Impedance Parameters

composites	R_{CT} (Ω)	R_{CT2} (Ω)
$Co_{[1.5]}Ni_{[3]}Fe_{[3]}$-LDH/$G_{[10]}$	188.10 ± 4.58	
CoNiFe-LDH	529.30 ± 4.58	
NiFe-LDH/G	354.70 ± 6.20	3673.0 ± 7.12
CoNi-LDH/G	511.50 ± 5.24	
CoFe-LDH/G	503.90 ± 5.83	

3673.0 ± 7.12 Ω. Furthermore, the CoNiFe-LDH without graphene has a higher R_{CT} of 529.30 ± 4.58 Ω. Consequently, the incorporation of G and Co into the $Co_{[1.5]}Ni_{[3]}Fe_{[3]}$-LDH/$G_{[10]}$ improves its electronic conductivity, expediting the charge transfer rate in the OER process.[74]

It is widely known that stability is a critical factor in determining whether electrocatalysts can be practically applied.[75] Therefore, the stability of the $Co_{[1.5]}Ni_{[3]}Fe_{[3]}$-LDH/$G_{[10]}$ was examined using chronoamperometry as a fixed potential of 1.58 V (RHE) equivalent to 10 mA cm^{-2}. The corresponding current−time plot is illustrated in Figure 8a. The current density decreases slightly to 9.48 mA cm^{-2} after 24 h due to the accumulation of bubbles on the active sites.[24] This indicates that there is only a negligible degradation in current density after a 24-h period, confirming that the $Co_{[1.5]}Ni_{[3]}Fe_{[3]}$-LDH/$G_{[10]}$ has advantageous durability and catalytic stability.

The stability was further evaluated using LSV curves, Figure 8b, and electrochemical impedance spectroscopy, Figure 8c, indicating differences before and after the stability test. While the onset potential is slightly improved after the 24 h period, there are more significant changes in the higher current densities. Additionally, the charge transfer resistance (R_{CT}) increases after the stability test from 188.1 to 424.1 Ω. The polarization of the catalyst at these high anodic potentials for the long-term of 24 h may cause its oxidation leading to some degradation of the $Co_{[1.5]}Ni_{[3]}Fe_{[3]}$-LDH/$G_{[10]}$ electronic conductivity.[75]

It is clear from Figure 7 that the graphene sheets facilitate the OER. However, in an alkaline environment, graphene sheets are susceptible to oxidation, especially at the potentials required for OER. To assess this, the stability of the graphene was compared with the graphene immobilized within the $Co_{[1.5]}Ni_{[3]}Fe_{[3]}$-LDH/$G_{[10]}$. Following a 24-h stability period at 1.58 V, cyclic voltammograms were recorded in a neutral phosphate buffer. The CV curves showed consistent behavior over 30 cycles, and the final cycles are plotted in Figure 8d. The two profiles exhibit distinct differences, particularly with the appearance of a peak at 0.4 V, indicative of graphene oxidation.[48] The absence of this peak at 0.4 V in the $Co_{[1.5]}Ni_{[3]}Fe_{[3]}$-LDH/$G_{[10]}$ CV profile indicates that the graphene maintained its structural integrity when incorporated into the composite. This enhanced stability is likely to be due

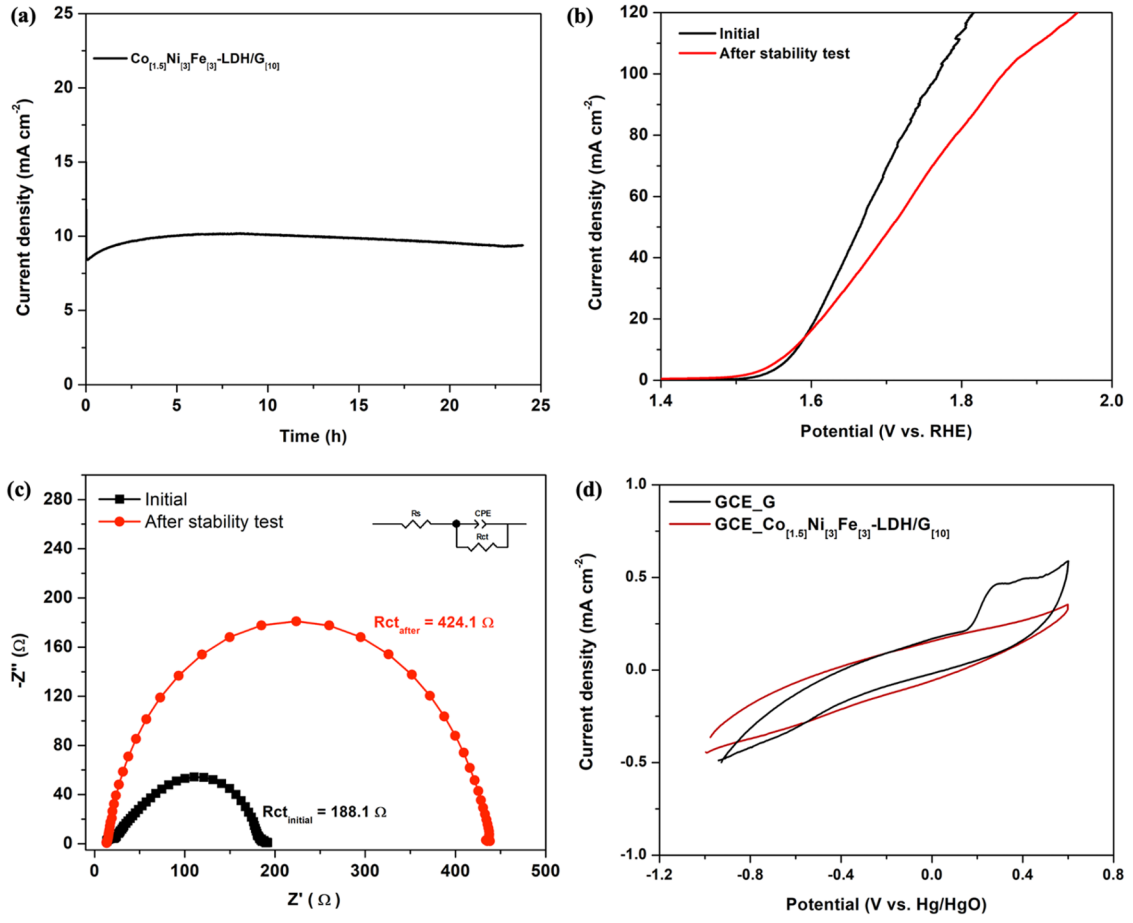

Figure 8. (a) A 24 h-stability test of $Co_{[1.5]}Ni_{[3]}Fe_{[3]}$-LDH/$G_{[10]}$ at 10 mA cm^{-2}, (b) polarization curves before and after stability test, (c) electrochemical impedance plot before and after stability test, and (d) CV in a buffer (pH 7.0) for graphene dispersed onto GCE and $Co_{[1.5]}Ni_{[3]}Fe_{[3]}$-LDH/$G_{[10]}$ after 24 h at 10 mA cm^{-2}.

https://doi.org/10.1021/acsaem.5c00483
ACS Appl. Energy Mater. 2025, 8, 5455−5467

to the protective effect of the LDH phase, which appears to effectively prevent oxidation of the graphene for at least 24 h.

It is well established that scaling up electrochemical systems typically requires higher current densities. Therefore, to evaluate the stability of the composite under such conditions over an extended duration, a chronoamperometry experiment was performed at a fixed potential of 1.66 V (RHE), corresponding to a current density of 50 mA cm^{-2}, for a period of 72 h. The resulting current−time profile shows an initial decrease in current density over the first 14 h, stabilizing at 44.5 mA cm^{-2}, as presented in Figure S3a. Beyond this period, the current density remained constant for the remaining 58 h, indicating that despite an initial decline, the composite maintained stability at 44.5 mA cm^{-2}. This stability was further supported by LSV curves recorded before and after the test, Figure S3b, which showed a slight increase in onset potential after 72 h, with more pronounced changes at higher current densities, as seen previously at 10 mA cm^{-2}.

Additionally, SEM was utilized to analyze the surface morphology of the composite both before and after the stability test, as shown in Figure S4a,b, respectively. Unlike the powder form of CoNiFe-LDH/G, the composite layer on GE exhibits a more compact morphology (Figure S4a) with minimal changes observed after the stability test (Figure S4b). This suggests that the material retains its morphology even under elevated current densities and prolonged operational conditions.

Furthermore, to evaluate potential metal leaching, the residual KOH solution after the 72 h stability test was analyzed using ICP. The elemental concentrations of Co, Ni, and Fe, expressed in ppb, are summarized in Table 8. The

Table 8. ICP-MS Analysis of Co, Ni, and Fe Concentrations in 1M KOH Solution Following a 72 h-Stability Test at 50 mA cm^{-2}

wavelength (nm)	Co (ppb)[a]	Ni (ppb)[a]	Fe (ppb)[a]
230.79	6.42 ± 0.03		
238.89	5.33 ± 0.02		
216.55		6.82 ± 0.06	
231.60		6.00 ± 0.02	
238.20			15.31 ± 0.33
261.19			9.19 ± 0.30

[a]Mean ± standard deviation (n = 3).

results indicate that the composite exhibits minimal metal leaching over the long-term test, as evidenced by the low concentrations of Co, Ni, and Fe in solution. Notably, Fe was detected at a higher concentration, which is consistent with the initial analysis of the unpurified KOH solution, where Fe impurities are present.

4. CONCLUSIONS

In this study, $Co_{[m]}Ni_{[3]}Fe_{[3]}$-LDH/$G_{[n]}$ composites were synthesized through a single-step hydrothermal reaction. The influence of cobalt and graphene concentrations on the OER performance was examined using a 2-level full factorial design to optimize the LDH composite for enhanced OER performance. The $Co_{[1.5]}Ni_{[3]}Fe_{[3]}$-LDH/$G_{[10]}$ composite reached the lowest onset potential of 1.54 V, the potential at 10 mA cm^{-2} was 1.58 V, and the Tafel slope was 58.4 mV dec^{-1}, indicating that a lower concentration of cobalt and graphene has the optimum combination for the OER process. Furthermore, the ANOVA analysis showed that both cobalt and graphene concentrations and their interactions are statistically significant, with a linear correlation between them. Also, the optimized composite showed good electronic properties and stability, without losing significant catalytic activity over a 24-h period. Additionally, the longer stability test at 50 mA cm^{-2} demonstrates a stable performance at 44.5 mA cm^{-2} for 58 h after an initial decline in current density. This stability was further supported by LSV analysis, which showed minor changes in onset potential and more significant changes in higher current density over 72 h. SEM imaging confirmed that the composite retains its compact morphology under prolonged operational conditions, while ICP-MS analysis indicated minimal metal leaching, with a slightly higher Fe concentration primarily attributed to impurities in the KOH solution. These findings highlight the composite's reliability for electrochemical applications under elevated current densities. Therefore, this study provides a facile and efficient strategy to design and optimize a trimetallic LDH combined with graphene as an electrocatalyst to enhance the OER activity.

■ ASSOCIATED CONTENT

Supporting Information

The Supporting Information is available free of charge at https://pubs.acs.org/doi/10.1021/acsaem.5c00483.

XPS of $Co_{[1.5]}Ni_{[3]}Fe_{[3]}$-LDH (a) Co 2p, (b) Ni 2p, (c) Fe 2p, and (d) O 1s (Figure S1); equivalent circuits of (a) CoNiFe-LDH/G, CoNiFe-LDH, CoNi-LDH/G, and CoFe-LDH/G; (b) NiFe-LDH/G (Figure S2); (a) 72 h-stability test of $Co_{[1.5]}Ni_{[3]}Fe_{[3]}$-LDH/$G_{[10]}$ at 50 mA cm^{-2}, (b) polarization curves before and after stability test (Figure S3); SEM images of $Co_{[1.5]}Ni_{[3]}Fe_{[3]}$-LDH/$G_{[10]}$ on the glassy carbon electrode: (a) before the stability test and (b) after the stability test at 50 mA cm^{-2} for 72 h (Figure S4) (PDF)

■ AUTHOR INFORMATION

Corresponding Author

Daniele Alves − *Department of Chemistry, Maynooth University, Maynooth, Co, Kildare W23 F2H6, Ireland;* orcid.org/0000-0001-6786-8638; Email: daniele.alves@mu.ie

Authors

Gillian Collins − *Department of Chemistry, Maynooth University, Maynooth, Co, Kildare W23 F2H6, Ireland*

Marilia B. Dalla Benetta − *Department of Chemistry, Maynooth University, Maynooth, Co, Kildare W23 F2H6, Ireland*

Eithne Dempsey − *Department of Chemistry and Kathleen Lonsdale Institute, Maynooth University, Maynooth, Co, Kildare W23 F2H6, Ireland*

Jae-Jin Shim − *School of Chemical Engineering, Yeungnam University, Gyeongsan 38541, Republic of Korea;* orcid.org/0000-0002-8027-9886

Raj Karthik − *Department of Chemistry, Maynooth University, Maynooth, Co, Kildare W23 F2H6, Ireland; School of Chemical Engineering, Yeungnam University, Gyeongsan 38541, Republic of Korea;* orcid.org/0000-0002-8605-643X

Carmel B. Breslin − *Department of Chemistry and Kathleen Lonsdale Institute, Maynooth University, Maynooth, Co,*

https://doi.org/10.1021/acsaem.5c00483
ACS Appl. Energy Mater. 2025, 8, 5455−5467

Kildare W23 F2H6, Ireland; orcid.org/0000-0002-0586-5375

Complete contact information is available at: https://pubs.acs.org/10.1021/acsaem.5c00483

Author Contributions

D.A.: Conceptualization, data curation, formal analysis, methodology, writing—original draft. G.C.: Validation, writing—review and editing. M.B.D.B.: Validation, writing—review and editing. E.D.: Data curation, supervision, writing—review and editing. R.K.: Writing—review and editing, formal analysis. J.-J.S.: Writing—review and editing, validation. C.B.B.: Project administration, resources, supervision, writing—original draft, writing—review and editing, validation.

Notes

The authors declare no competing financial interest.

■ ACKNOWLEDGMENTS

This publication has emanated from research conducted with the financial support of Research Ireland, under Grant numbers SFI/20/FFP-P/8793 and IRC/GOIPG/2022/1605, and the Sustainability Energy Authority of Ireland, grant number SEAI/22/RDD/841.

■ REFERENCES

(1) Hirsh, R. F.; Koomey, J. G. Electricity Consumption and Economic Growth: A New Relationship with Significant Consequences? *Electr. J.* **2015**, *28* (9), 72−84.

(2) Chen, X. H.; Tee, K.; Elnahass, M.; Ahmed, R. Assessing the Environmental Impacts of Renewable Energy Sources: A Case Study on Air Pollution and Carbon Emissions in China. *J. Environ. Manage.* **2023**, *345*, No. 118525.

(3) Su, C. W.; Mirza, N.; Umar, M.; Chang, T.; Albu, L. L. Resource Extraction, Greenhouse Emissions, and Banking Performance. *Resour. Policy* **2022**, *79*, No. 103122.

(4) Ahmed, J.; Ahamad, T.; Alhokbany, N.; Majeed Khan, M. A.; Arunachalam, P.; Amer, M. S.; Alotaibi, R. M.; Alshehri, S. M. Reduced Graphene Oxide Encapsulated Perovskite-Type Lanthanum Cobalt Oxide Nanoparticles for Efficient Electrolysis of Water to Oxygen Reactions (OER/ORR). *J. Ind. Eng. Chem.* **2023**, *121*, 100−106.

(5) Lim, J.; Jung, J. W.; Kim, N. Y.; Lee, G. Y.; Lee, H. J.; Lee, Y.; Choi, D. S.; Yoon, K. R.; Kim, Y. H.; Kim, I. D.; Kim, S. O. N2-Dopant of Graphene with Electrochemically Switchable Bifunctional ORR/OER Catalysis for Zn-Air Battery. *Energy Storage Mater.* **2020**, *32*, 517−524.

(6) Li, J.; Qian, J.; Chen, X.; Zeng, X.; Li, L.; Ouyang, B.; Kan, E.; Zhang, W. Three-Dimensional Hierarchical Graphitic Carbon Encapsulated CoNi Alloy/N-Doped CNTs/Carbon Nanofibers as an Efficient Multifunctional Electrocatalyst for High-Performance Microbial Fuel Cells. *Composites, Part B* **2022**, *231*, No. 109573.

(7) Zeng, F.; Mebrahtu, C.; Liao, L.; Beine, A. K.; Palkovits, R. Stability and Deactivation of OER Electrocatalysts: A Review. *J. Energy Chem.* **2022**, *69*, 301−329.

(8) Chen, M.; Wang, L.; Yang, H.; Zhao, S.; Xu, H.; Wu, G. Nanocarbon/Oxide Composite Catalysts for Bifunctional Oxygen Reduction and Evolution in Reversible Alkaline Fuel Cells: A Mini Review. *J. Power Sources* **2018**, *375*, 277−290.

(9) Qian, J.; Zhang, Y.; Chen, Z.; Du, Y.; Ni, B. J. NiCo Layered Double Hydroxides/NiFe Layered Double Hydroxides Composite (NiCo-LDH/NiFe-LDH) towards Efficient Oxygen Evolution in Different Water Matrices. *Chemosphere* **2023**, *345*, No. 140472.

(10) He, S.; Yue, R.; Liu, W.; Ding, J.; Zhu, X.; Liu, N.; Guo, R.; Mo, Z. Nano-NiFe LDH Assembled on CNTs by Electrostatic Action as an Efficient and Durable Electrocatalyst for Oxygen Evolution. *J. Electroanal. Chem.* **2023**, *946*, No. 117718.

(11) Rezvani, Z.; Foruzin, L. J.; Nejati, K.; Dai, H. Nest-like NiFe-LDH Derived from the Ethylene Glycol-Assisted Hydrothermal Route: A Highly Efficient Electrocatalyst for Water Oxidation in Neutral Solutions. *Appl. Clay Sci.* **2023**, *246*, No. 107195.

(12) Liu, D.; Yang, Y.; Zhang, J.; Wang, L.; Ma, Z.; Ren, L.; Wang, J.; Xue, B.; Li, F. Improved OER Catalytic Performance of NiFe-LDH with Hydrothermal Carbonization Microspheres. *J. Alloys Compd.* **2023**, *941*, No. 168994.

(13) Wang, S.; Wang, T.; Wang, X.; Deng, Q.; Yang, J.; Mao, Y.; Wang, G. Intercalation and Elimination of Carbonate Ions of NiCo Layered Double Hydroxide for Enhanced Oxygen Evolution Catalysis. *Int. J. Hydrogen Energy* **2020**, *45* (23), 12629−12640.

(14) Alves, D.; Moral, R. A.; Jayakumari, D.; Dempsey, E.; Breslin, C. B. Factorial Optimization of CoCuFe-LDH/Graphene Ternary Composites as Electrocatalysts for Water Splitting. *ACS Appl. Mater. Interfaces* **2024**, *16* (38), 50846−50858.

(15) Raja, A.; Son, N.; Kim, Y. Il.; Kang, M. Hybrid Ternary NiCoCu Layered Double Hydroxide Electrocatalyst for Alkaline Hydrogen and Oxygen Evolution Reaction. *J. Colloid Interface Sci.* **2023**, *647*, 104−114.

(16) Liao, F.; Yang, G.; Cheng, Q.; Mao, L.; Zhao, X.; Chen, L. Rational Design and Facile Synthesis of Ni-Co-Fe Ternary LDH Porous Sheets for High-Performance Aqueous Asymmetric Supercapacitor. *Electrochim. Acta* **2022**, *428*, No. 140939.

(17) Cao, S.; Lu, X.; Gong, P.; Quan, C.; Fan, X.; Yang, Z. Co-Doped NiFe-LDH Nanosheets Arrays Supported on Nickel Foam as an Efficient Oxygen Evolution Electrocatalysis. *J. Electroanal. Chem.* **2023**, *948*, No. 117825.

(18) Wu, G.; Santandreu, A.; Kellogg, W.; Gupta, S.; Ogoke, O.; Zhang, H.; Wang, H. L.; Dai, L. Carbon Nanocomposite Catalysts for Oxygen Reduction and Evolution Reactions: From Nitrogen Doping to Transition-Metal Addition. *Nano Energy* **2016**, *29*, 83−110.

(19) Xie, J.; Li, C.; Niu, J.; Zhang, S.; Ou, X.; Feng, P.; Garcia, H. Porous NiFe-LDH Grown on Graphene Oxide towards Highly Efficient OER Electrocatalysis. *Mater. Lett.* **2021**, *290*, No. 129517.

(20) Zhong, H.; Cheng, X.; Xu, H.; Li, L.; Li, D.; Tang, P.; Alonso-Vante, N.; Feng, Y. Carbon Fiber Paper Supported Interlayer Space Enlarged Ni2Fe-LDHs Improved OER Electrocatalytic Activity. *Electrochim. Acta* **2017**, *258*, 554−560.

(21) Ji, K.; Xia, X.; Yue, Y.; Yang, P. Nanoarchitectonics with NiFe-Layered Double Hydroxide Decorated Co/Ni-Carbon Nanotubes for Efficient Oxygen Evolution Reaction Electrocatalysis. *J. Electroanal. Chem.* **2022**, *920*, No. 116573.

(22) Yuan, F.; Wei, J.; Qin, G.; Ni, Y. Carbon Cloth Supported Hierarchical Core-Shell NiCo2S4@CoNi-LDH Nanoarrays as Catalysts for Efficient Oxygen Evolution Reaction in Alkaline Solution. *J. Alloys Compd.* **2020**, *830*, No. 154658.

(23) Gao, W.; Havas, D.; Gupta, S.; Pan, Q.; He, N.; Zhang, H.; Wang, H. L.; Wu, G. Is Reduced Graphene Oxide Favorable for Nonprecious Metal Oxygen-Reduction Catalysts? *Carbon* **2016**, *102*, 346−356.

(24) Song, S.; Fu, Y.; Yin, F.; Zhang, Y.; Ma, J.; Liu, Y.; Ren, J.; Ye, W.; Ma, R. NiFe-Based Tungstate@layered Double Hydroxide Heterostructure Supported on Graphene as Efficient Oxygen Evolution Reaction Catalyst. *Mater. Today Chem.* **2023**, *28*, No. 101369.

(25) Gu, Y.; Yang, Z.; Zhou, J.; Chen, Z. Application of Graphene/LDH in Energy Storage and Conversion. *Sustainable Mater. Technol.* **2023**, *37*, No. e00695.

(26) Liang, J.; Wei, Y.; Yao, Y.; Zheng, X.; Shen, J.; He, G.; Chen, H. Constructing High-Efficiency Photocatalyst for Degrading Ciprofloxacin: Three-Dimensional Visible Light Driven Graphene Based NiAlFe LDH. *J. Colloid Interface Sci.* **2019**, *540*, 237−246.

(27) Khalili, R.; Sabzehmeidani, M. M.; Parvinnia, M.; Ghaedi, M. Removal of Hexavalent Chromium Ions and Mixture Dyes by Electrospun PAN/Graphene Oxide Nanofiber Decorated with

Bimetallic Nickel−Iron LDH. *Environ. Nanotechnol. Monit. Manage.* **2022**, *18*, No. 100750.
(28) Wang, X.; Wang, Q.; Hou, X.; Liu, Y.; Zheng, P.; Huo, J.; Yin, L.; Guo, S. Facile Fabrication of Two-Dimensional Reduced Graphene Oxide/CoAl-Layered Double Hydroxides Nanocomposites for Lithium-Oxygen Battery with Improved Electrochemical Performance. *J. Alloys Compd.* **2018**, *744*, 196−203.
(29) Subbaraman, R.; Danilovic, N.; Lopes, P. P.; Tripkovic, D.; Strmcnik, D.; Stamenkovic, V. R.; Markovic, N. M. Origin of Anomalous Activities for Electrocatalysts in Alkaline Electrolytes. *J. Phys. Chem. C* **2012**, *116* (42), 22231−22237.
(30) Trotochaud, L.; Young, S. L.; Ranney, J. K.; Boettcher, S. W. Nickel-Iron Oxyhydroxide Oxygen-Evolution Electrocatalysts: The Role of Intentional and Incidental Iron Incorporation. *J. Am. Chem. Soc.* **2014**, *136* (18), 6744−6753.
(31) Márquez, R. A.; Kawashima, K.; Son, Y. J.; Castelino, G.; Miller, N.; Smith, L. A.; Chukwuneke, C. E.; Mullins, C. B. Getting the Basics Right: Preparing Alkaline Electrolytes for Electrochemical Applications. *ACS Energy Lett.* **2023**, *8* (2), 1141−1146.
(32) Fei, H.; Dong, J.; Arellano-Jiménez, M. J.; Ye, G.; Dong Kim, N.; Samuel, E. L. G.; Peng, Z.; Zhu, Z.; Qin, F.; Bao, J.; Yacaman, M. J.; Ajayan, P. M.; Chen, D.; Tour, J. M. Atomic Cobalt on Nitrogen-Doped Graphene for Hydrogen Generation. *Nat. Commun.* **2015**, *6*, No. 8668.
(33) Zhuo, H. Y.; Zhang, X.; Liang, J. X.; Yu, Q.; Xiao, H.; Li, J. Theoretical Understandings of Graphene-Based Metal Single-Atom Catalysts: Stability and Catalytic Performance. *Chem. Rev.* **2020**, *120* (21), 12315−12341.
(34) Luo, J.; Jang, H. D.; Huang, J. Effect of Sheet Morphology on the Scalability of Graphene-Based Ultracapacitors. *ACS Nano* **2013**, *7* (2), 1464−1471.
(35) Wang, Q.; Yu, Z.; Liu, Y.; Zhu, X.; Long, R.; Li, X. Electrostatic Self-Assembly Method to Prepare Intercalated Graphene Oxide Composite Membrane to Improve Hydrophilicity and Flux. *Diamond Relat. Mater.* **2021**, *117*, No. 108492.
(36) Shivakumar, P.; Monika, M. N.; Deepu, M.; Manjunatha kumara, K. S.; Budagumpi, S.; Nagaraju, D. H. Amorphous and Crystalline Heterostructure MoSe2/NiFe-LDH through p-n Junction Formation for Electrochemical Water Splitting-Synergistic Back Bonding Effect. *Int. J. Hydrogen Energy* **2024**, *65*, 74−82.
(37) Nayak, S.; Parida, K. Plasmon-Induced Electron Transportation in Heterostructure N-RGO/NiFe-LDH@Au with Enhanced Photoelectrochemical Water Oxidation. *Electrochim. Acta* **2024**, *500*, No. 144724.
(38) Zhang, Y.; Liu, H.; Zhu, P.; Yang, M.; Jin, Z. In Situ XPS Proved Effective Charge Transfer over ZIF-67@CoFe LDH S-Scheme Heterojunctions for Efficient Visible Light Driven Hydrogen Evolution. *Int. J. Hydrogen Energy* **2023**, *48* (84), 32631−32641.
(39) Elshishini, H. M.; Elsubruiti, G. M.; Ghatass, Z. F.; Eltaweil, A. S. Microwave-Assisted Synthesis of Zn−Fe LDH Modified with Magnetic Oxidized Hydrochar for Pb(II) Removal: Insights into Stability, Performance and Mechanism. *J. Solid State Chem.* **2024**, *335*, No. 124689.
(40) Pei, Y.; Ge, Y.; Chu, H.; Smith, W.; Dong, P.; Ajayan, P. M.; Ye, M.; Shen, J. Controlled Synthesis of 3D Porous Structured Cobalt-Iron Based Nanosheets by Electrodeposition as Asymmetric Electrodes for Ultra-Efficient Water Splitting. *Appl. Catal., B* **2019**, *244*, 583−593.
(41) Hui, L.; Xue, Y.; Huang, B.; Yu, H.; Zhang, C.; Zhang, D.; Jia, D.; Zhao, Y.; Li, Y.; Liu, H.; Li, Y. Overall Water Splitting by Graphdiyne-Exfoliated and -Sandwiched Layered Double-Hydroxide Nanosheet Arrays. *Nat. Commun.* **2018**, *9* (1), No. 5309.
(42) Hu, S.; Tan, Y.; Feng, C.; Wu, H.; Zhang, J.; Mei, H. Synthesis of N Doped NiZnCu-Layered Double Hydroxides with Reduced Graphene Oxide on Nickel Foam as Versatile Electrocatalysts for Hydrogen Production in Hybrid-Water Electrolysis. *J. Power Sources* **2020**, *453*, No. 227872.
(43) Bhavanari, M.; Lee, K. R.; Tseng, C. J.; Su, B. J.; Chen, J. M.; Chang, J. K.; Bhattacharyya, A. J.; Su, C. Y. New Insights into Interface Charge-Transfer Mechanism of Copper-Iron Layered Double Hydroxide Cathodic Electrocatalyst in Alkaline Electrolysis. *J. Environ. Chem. Eng.* **2022**, *10* (2), No. 107287.
(44) Song, Y.; Xu, B.; Liao, T.; Guo, J.; Wu, Y.; Sun, Z. Electronic Structure Tuning of 2D Metal (Hydr)Oxides Nanosheets for Electrocatalysis. *Small* **2021**, *17* (9), No. 2002240.
(45) Nayak, S.; Parida, K. Recent Progress in LDH@Graphene and Analogous Heterostructures for Highly Active and Stable Photocatalytic and Photoelectrochemical Water Splitting. *Chem. - Asian J.* **2021**, *16* (16), 2211−2248.
(46) Shen, G.; Zhang, L.; Gu, Z.; Zheng, Z.; Liu, Y.; Tan, G.; Jie, X. Zinc Aluminum-Layered Double Hydroxide(LDH)-Graphene Oxide-(GO) Lubricating and Corrosion-Resistant Composite Coating on the Surface of Magnesium Alloy. *Surf. Coat. Technol.* **2022**, *437*, No. 128354.
(47) Zhang, Y.; Yu, P.; Wang, J.; Li, Y.; Chen, F.; Wei, K.; Zuo, Y. LDHs/Graphene Film on Aluminum Alloys for Active Protection. *Appl. Surf. Sci.* **2018**, *433*, 927−933.
(48) Banou, M.; Niu, Y.; Ammari, F.; Dunlop, T.; Palmer, R. E.; Tizaoui, C. Fabrication of Graphene Nanoplatelets/MgAl-Layered Double Hydroxide Nanocomposites as Efficient Support for Gold Nanoparticles and Their Catalytic Performance in 4-Nitrophenol Reduction. *Process Saf. Environ. Prot.* **2023**, *174*, 891−900.
(49) Xia, D. C.; Zhou, L.; Qiao, S.; Zhang, Y.; Tang, D.; Liu, J.; Huang, H.; Liu, Y.; Kang, Z. Graphene/Ni-Fe Layered Double-Hydroxide Composite as Highly Active Electrocatalyst for Water Oxidation. *Mater. Res. Bull.* **2016**, *74*, 441−446.
(50) Wang, Q.; Chen, L.; Guan, S.; Zhang, X.; Wang, B.; Cao, X.; Yu, Z.; He, Y.; Evans, D. G.; Feng, J.; Li, D. Ultrathin and Vacancy-Rich CoAl-Layered Double Hydroxide/Graphite Oxide Catalysts: Promotional Effect of Cobalt Vacancies and Oxygen Vacancies in Alcohol Oxidation. *ACS Catal.* **2018**, *8* (4), 3104−3115.
(51) Zhang, M.; Li, Y.; Yan, X.; Zhang, W.; Huang, X.; Pan, J.; Shahnavaz, Z. Construction of NiCo-LDH Vertical Standing Arrays on Carbon Fibers for Highly Effective Supercapacitors and Catalytic Oxygen Evolution Applications. *J. Alloys Compd.* **2023**, *934*, No. 167955.
(52) Gholami, P.; Heidari, A.; Khataee, A.; Ritala, M. Oxygen and Nitrogen Plasma Modifications of ZnCuCo LDH-Graphene Nanocomposites for Photocatalytic Hydrogen Production and Antibiotic Degradation. *Sep. Purif. Technol.* **2023**, *325*, No. 124706.
(53) Huang, L.; Liu, B.; Hou, H.; Wu, L.; Zhu, X.; Hu, J.; Yang, J. Facile Preparation of Flower-like NiMn Layered Double Hydroxide/Reduced Graphene Oxide Microsphere Composite for High-Performance Asymmetric Supercapacitors. *J. Alloys Compd.* **2018**, *730*, 71−80.
(54) Nayak, S.; Mohapatra, L.; Parida, K. Visible Light-Driven Novel g-C3N4/NiFe-LDH Composite Photocatalyst with Enhanced Photocatalytic Activity towards Water Oxidation and Reduction Reaction. *J. Mater. Chem. A* **2015**, *3* (36), 18622−18635.
(55) Chen, Q.; Pan, H.; Chen, Z.; Jiang, X.; Li, Y.; Tian, W.; Liu, H.; Zhu, S. Cobalt Coordinated Carbon Quantum Dots Boosting the Performance of NiCo-LDH for Energy Storage. *J. Colloid Interface Sci.* **2024**, *655*, 110−119.
(56) Kooravand, M.; Haddadi, H.; Asadpour, S.; Farhadian, S.; Sarmast, N.; Asfaram, A. Simply Synthesized Ca-Al-LDH-Thiosulfate as Adsorbent for Removal of Malachite Green from Aqueous Solution. *Polyhedron* **2023**, *246*, No. 116653.
(57) Çiplak, Z.; Yildiz, N.; Çalimli, A. Investigation of Graphene/Ag Nanocomposites Synthesis Parameters for Two Different Synthesis Methods. *Fullerenes, Nanotubes Carbon Nanostruct.* **2015**, *23* (4), 361−370.
(58) Shen, J.; Shi, M.; Li, N.; Yan, B.; Ma, H.; Hu, Y.; Ye, M. Facile Synthesis and Application of Ag-Chemically Converted Graphene Nanocomposite. *Nano Res.* **2010**, *3* (5), 339−349.
(59) Zhang, Q.; Xie, Y.; Ling, F.; Song, Z.; Li, D.; Lu, Y.; Tang, X.; Li, Y.; Zhou, X. Bimetallic Nickel-Cobalt Oxides: A Comprehensive Insight into Ni/Co Ratio, Intrinsic Structure and Electrochemical Behaviors. *Vacuum* **2022**, *196*, No. 110764.

https://doi.org/10.1021/acsaem.5c00483
ACS Appl. Energy Mater. 2025, 8, 5455−5467

(60) Bates, M. K.; Jia, Q.; Doan, H.; Liang, W.; Mukerjee, S. Charge-Transfer Effects in Ni-Fe and Ni-Fe-Co Mixed-Metal Oxides for the Alkaline Oxygen Evolution Reaction. *ACS Catal.* **2016**, *6* (1), 155−161.
(61) Feng, L.; Li, A.; Li, Y.; Liu, J.; Wang, L.; Huang, L.; Wang, Y.; Ge, X. A Highly Active CoFe Layered Double Hydroxide for Water Splitting. *ChemPlusChem* **2017**, *82* (3), 483−488.
(62) Lin, Y.; Wang, H.; Peng, C. K.; Bu, L.; Chiang, C. L.; Tian, K.; Zhao, Y.; Zhao, J.; Lin, Y. G.; Lee, J. M.; Gao, L. Co-Induced Electronic Optimization of Hierarchical NiFe LDH for Oxygen Evolution. *Small* **2020**, *16* (38), No. 2002426.
(63) Baig, Z.; Mamat, O.; Mustapha, M. Recent Progress on the Dispersion and the Strengthening Effect of Carbon Nanotubes and Graphene-Reinforced Metal Nanocomposites: A Review. *Crit. Rev. Solid State Mater. Sci.* **2018**, *43* (1), 1−46.
(64) Lobinsky, A. A.; Tolstoy, V. P. Synthesis of CoAl-LDH Nanosheets and N-Doped Graphene Nanocomposite via Successive Ionic Layer Deposition Method and Study of Their Electrocatalytic Properties for Hydrogen Evolution in Alkaline Media. *J. Solid State Chem.* **2019**, *270*, 156−161.
(65) Zhang, L.; Yao, H.; Li, Z.; Sun, P.; Liu, F.; Dong, C.; Wang, J.; Li, Z.; Wu, M.; Zhang, C.; Zhao, B. Synthesis of Delaminated Layered Double Hydroxides and Their Assembly with Graphene Oxide for Supercapacitor Application. *J. Alloys Compd.* **2017**, *711*, 31−41.
(66) Xu, H.; Wang, B.; Shan, C.; Xi, P.; Liu, W.; Tang, Y. Ce-Doped NiFe-Layered Double Hydroxide Ultrathin Nanosheets/Nanocarbon Hierarchical Nanocomposite as an Efficient Oxygen Evolution Catalyst. *ACS Appl. Mater. Interfaces* **2018**, *10* (7), 6336−6345.
(67) Tang, D.; Han, Y.; Ji, W.; Qiao, S.; Zhou, X.; Liu, R.; Han, X.; Huang, H.; Liu, Y.; Kang, Z. A High-Performance Reduced Graphene Oxide/ZnCo Layered Double Hydroxide Electrocatalyst for Efficient Water Oxidation. *Dalton Trans.* **2014**, *43* (40), 15119−15125.
(68) Lu, Z.; Li, Q.; Yang, T.; Yaping, L.; Xiaoming, S.; Xue, D. Ternary NiFeMn Layered Double Hydroxides as Highly-Efficient Oxygen Evolution Catalysts. *Chem. Commun.* **2016**, *52* (5), 908−911.
(69) Carrasco, J. A.; Harvey, A.; Hanlon, D.; Lloret, V.; McAteer, D.; Sanchis-Gual, R.; Hirsch, A.; Hauke, F.; Abellán, G.; Coleman, J. N.; Coronado, E. Liquid Phase Exfoliation of Carbonate-Intercalated Layered Double Hydroxides. *Chem. Commun.* **2019**, *55* (23), 3315−3318.
(70) Ge, R.; Ren, X.; Ji, X.; Liu, Z.; Du, G.; Asiri, A. M.; Sun, X.; Chen, L. Benzoate Anion-Intercalated Layered Cobalt Hydroxide Nanoarray: An Efficient Electrocatalyst for the Oxygen Evolution Reaction. *ChemSusChem* **2017**, *10* (20), 4004−4008.
(71) Nejati, K.; Davari, S.; Akbari, A.; Asadpour-Zeynali, K.; Rezvani, Z. A Highly Active Oxygen Evolution Electrocatalyst: Ni-Fe-Layered Double Hydroxide Intercalated with the Molybdate and Vanadate Anions. *Int. J. Hydrogen Energy* **2019**, *44* (29), 14842−14852.
(72) Jia, X.; Zhang, X.; Zhao, J.; Zhao, Y.; Zhao, Y.; Waterhouse, G. I. N.; Shi, R.; Wu, L. Z.; Tung, C. H.; Zhang, T. Ultrafine Monolayer Co-Containing Layered Double Hydroxide Nanosheets for Water Oxidation. *J. Energy Chem.* **2019**, *34*, 57−63.
(73) Sanchis-Gual, R.; Seijas-Da Silva, A.; Coronado-Puchau, M.; Otero, T. F.; Abellán, G.; Coronado, E. Improving the Onset Potential and Tafel Slope Determination of Earth-Abundant Water Oxidation Electrocatalysts. *Electrochim. Acta* **2021**, *388*, No. 138613.
(74) Ray, P. K.; Mohanty, R.; Parida, K. Recent Advancements of NiCo LDH and Graphene Based Nanohybrids for Supercapacitor Application. *J. Energy Storage* **2023**, *72*, No. 108335.
(75) Maljusch, A.; Conradi, O.; Hoch, S.; Blug, M.; Schuhmann, W. Advanced Evaluation of the Long-Term Stability of Oxygen Evolution Electrocatalysts. *Anal. Chem.* **2016**, *88* (88), 7597−7602.

https://doi.org/10.1021/acsaem.5c00483
ACS Appl. Energy Mater. 2025, 8, 5455−5467